Regular Article

Check for
updates

Heat transfer characteristics of moving longitudinal porous fin wetted with ternary (Cu–Al$_2$O$_3$–TiO$_2$) hybrid nanofluid: ADM solution

Mehdi Ouada[1], **Mohamed Kezzar**[2], **Nabil Talbi**[2], **Mohamed R. Eid**[3,4,a], **Mohamed Rafik Sari**[5], **W. M. Yousef**[6,7], **Essam M. Elsaid**[8,9]

[1] Electromechanical Department, LSEM Laboratory, University Badji Mokhtar, Annaba, Algeria
[2] Mechanical Engineering Department, University of Skikda, El Hadaiek Road, B.O. 26, 21000 Skikda, Algeria
[3] Department of Mathematics, Faculty of Science, New Valley University, El-Kharga, Al-Wadi Al-Gadid 72511, Egypt
[4] Finance and Insurance Department, College of Business Administration, Northern Border University, 1321 Arar, Saudi Arabia
[5] Mechanics of Materials and Plant Maintenance Research Laboratory (LR3MI), Mechanical Engineering Department, Faculty of Engineering, Badji Mokhtar University of Annaba (UBMA), PO Box 12, 23052 Annaba, Algeria
[6] Mathematical Sciences Department, College of Science, United Arab Emirates University, P.O. Box No. 15551, Al Ain, UAE
[7] Basic Science Department, Canadian International College for Engineering, Cairo, Egypt
[8] Department of Mathematics, College of Science, University of Bisha, P.O. Box 344, 61922 Bisha, Saudi Arabia
[9] Basic Sciences Department, El Gazeera High Institute for Engineering and Technology, Cairo, Egypt

Abstract In this work, a numerical and analytical investigation of the heat transfer processes of free convection and radiation on a porous moving longitudinal fin has been carried out. A ternary hybridized nanofluid consisting of Cu, Al$_2$O$_3$, and TiO$_2$ is being used to wet the moving fin in this case. Both the pure water (H$_2$O) as a base fluid, and once again the combination of water + C$_2$H$_6$O$_2$ (50–50%) as a base fluid, are taken into consideration. In the process of modeling the current physical phenomena, Darcy's model is being taken into consideration. The primary equations were solved by using a technique known as the Adomian decomposition method (ADM). This solution was then verified by utilizing the HAM-based Mathematica package known as BVPh 2 as well as Runge–Kutta–Fehlberg fourth–fifth-order (RKF-45) approach. The impacts of a variety of different factors on thermal profiles and thermal gradients are depicted and analyzed. These parameters include nanoparticle volume fraction, Peclet number, wet porosity, radiative parameter, convective number, power index, and ambient temperature on ternary hybrid nanofluid is another parameter that influences thermal profiles and thermal gradients.

List of symbols

Cu	Copper
Al$_2$O$_3$	Aluminum (III) oxide
TiO$_2$	Titanium dioxide
H$_2$O	Water
C$_2$H$_6$O$_2$	Ethylene glycol
Thnf	Ternary hybrid nanofluid
nf	Nanofluid
f	Fluid
a	Constant
$\overline{\varphi}$	Porosity
Pe	Peclet number
l	Fin length (m)
T_a	Ambient temperature (K)
T	Temperature (K)
μ	Dynamic viscosity (kg/ms)
ρ	Density (kg/m^3)
C_p	Specific heat (J/kg · K)
β	Thermal expansion coefficient

[a] e-mail: m_r_eid@yahoo.com (corresponding author)

k	Thermal conductivity (W/mK)
K	Penetrability (N/A^2)
b_2	Fin variant factor (1/K)
ω	Filled air moisture radio
ω_a	Surrounding air moisture
U	Uniform velocity (m/s)
t	Fin thickness
w	Fin width (m)
h	Heat transmission factor at T_a (W/m^{2}K)
h_D	Uniform mass transference factor
θ	Nondimensional temperature
g	Gravity acceleration (m/s^2)
θ_a	Nondimensional ambient temperature
T_b	Fin temperature
η	Dimensionless axial distance
Nr	Radiation parameter
φ_1	Factional size of Cu
φ_2	Factional size of Al$_2$O$_3$
φ_3	Factional size of TiO$_2$
Nc	Convective number
m_2	Wet porous number ($= m_0 + m_1$)
n	Power-index
m_0, m_1	Constants
x	Coordinate (m)
σ	Stefan-Boltzmann constant (W/m^{2}K^4)
ε	Fin material emissivity
ν	Kinematic viscosity (m^2/s)
φ	Fractional size of nanoparticles

1 Introduction

Nanofluid is a term used to describe any fluid that contains nanoparticles. These liquids are nanoparticle dispersion in a designed colloidal solution. Nanomaterials can be nanoparticles, nanowires, nanotubes, or nanofibers, and the main fluid can be water, oil, biological fluids, lubricants, organic liquids (coolants, ethylene glycol, ethylene, or polymer solutions), or regular fluid. Nano-liquid is made when any of the above unique materials are mixed with the base liquid. Metal oxides (like MgO, SiO$_2$, and TiO$_2$), ceramic oxides (like Al$_2$O$_3$, Be$_2$O$_3$, and CuO), chemically stable metals (like gold and copper), different types of carbon (like diamonds, graphite, and carbonless nanotubes (Fullerene)), solid minerals (like SiC), and functional nanoparticles are all commonly used as nanoparticles [1–3].

Heat transfer is utilized to enhance thermal efficiency and cooling systems in a variety of industrial, engineering, and medical applications. Nanofluids have been found to have higher thermal conductivity and adsorption capacity than regular fluids. Because of this, nanoparticles are being used as a desirable material in the development of fluids to maximize heat transfer in automated manufacturing systems such as cooling electronic circuits and heat exchangers, and cooling heat exchange mechanisms in processors, metal tapes and radiators, car engines, welding equipment, cooling chemical reactions and car cooling systems, fuel cells, and cancer therapy [4, 5].

The ternary hybrid nanofluid is a novel term that has emerged in recent years as a result of the influence of these liquids on flow and heat transport attributes. This combination formed between molecules after extensive investigation demonstrated the influence of nanofluids on movement and heat transference capabilities [6–9].

After a lot of research into how nanoparticles affect the properties of regular fluids, it was suggested that more types of nanoparticles should be employed to improve the performing of fluid properties in manufacturing or organic settings [10–13]. Another key component that aids in heat transmission is the tying of the enlarged surface, which is the fin, to the old structure. This increases the surface available for heat transfer and, as a result, improves the cooling effect.

Gireesha et al. [14] examined heat transmission via a constant-velocity longitudinal fin and fin tip convection in a hybrid nanomaterial flow. Talbi et al. [15] observed the effects of thermic radiation and natural convection on the flowing of a hybridized nanoliquid (H$_2$O–C$_2$H$_6$O$_2$/GO–MoS$_2$) across a moving porous longitudinal fin using insulated and convective boundary conditions. Kezzar et al. [16] introduced a novel analytical computer methodology dubbed the Duan–Rach method (DRA) to examine longitudinal fin heat transmission with thermal conductance and temperature-dependent heat generating. Sowmya et al. [17] increased heat transfer rates in convective boundary conditions and inside heat generating using alloy-embedded nanoliquid flowing and porousness fin in

wet conditions with natural convection and radiation. Goud et al. [18] employed a ternary hybrid nanofluid to observe heat transport through a totally wet dovetail fin, considering the temperature and humidity ratio. Hosseinzadeh et al. [19] analyzed the thermal efficacy of a movable porous fin moistened with a hybridized nanoliquid of varying cross sections in a magnetized force. For a longitudinal fin with a heat source and constant rapidity, Gouran et al. [20] studied convection and radiation heat transfer using LSM and MOM techniques.

When it comes to similar inertia effects, the Darcy–Forchheimer model is the most common change to the Darcy flow. The consequence of inertia is considered by the Forchheimer extension, which adds a velocity-squared factor to the momentum equation. Studying the two-dimensional Darcy–Forchheimer motion of magnetized Maxwell liquid created by a linearly stretched surface and convective heat transfer was the focus of Sadiq and Hayat [21] research. In their investigation of generalized Forchheimer flows in porous media, Ibragimov and Kiu [22] made use of an enlarged mixed finite element approach. The heat radiation in a 3D Darcy–Forchheimer rotating flow of MHD CNTs nanofluid was studied by Shah et al. [23] who conducted their research between parallel plates. The Darcy–Forchheimer viscous fluid flow over a curving extended plate was investigated by Hayat and Saif [24]. Entropy optimization in the Darcy–Forchheimer flowing of first-order slippage rapidity of the Carreau–Yasuda liquid was computed by Khan et al. [25]. Modeling the flow of a Darcy–Forchheimer hybrid nanofluid with partial slip across a spinning disk was accomplished by Li et al. [26] by using the technique of fractional simulation. Elsaid and Abdel-Aal [27] investigated the energy and mass features of a mixed convective flow of nanofluid via a porous plate that was implanted in a porous medium when a magnetic field and heat radiation were present. Their research focused on the movement of nanoliquid through the porosity plate.

The increase in heat transmission has been investigated using a wide number of approaches, and one of the most successful of these approaches is the fin technique, which examines the heat transfer properties of a system [28, 29]. Fins are often used in a wide variety of manufacturing processes to facilitate heat transmission. These applications include heat exchangers as well as microchannel heat sinks [30]. Numerous processes used in industry, including extrusion, hot rolling, and casting, apply a thermal treatment to the material that is being developed and manufactured while it is in continuous movement. This treatment is often carried out in comparison with the fluid that is surrounding the material being produced [31]. This makes it possible to get the material down to the correct temperature and cool it. The sheet area of the substance is increased by using fins that have been stretched into the environment that surrounds it. This helps to enhance the impact of cooling. Fins are solids that extend from an item to expand the heat transport rate and assist disperse heat from a hot sheet into the environment around it. Fins may be found on heat sinks, radiators, and other devices designed to transfer heat [32]. An examination of the previous research reveals that extensive effort has been done in the investigation of a variety of different types of fin designs [33–35]. When the cooling impact is provided by the wetted situation, heat dissipation is more efficient, and the usage of increased surfaces under moist circumstances is more prominent in cooling and refrigeration systems. Under these conditions, simultaneous heat transmission and mass transfer take place over the surface of the fin that is associated with the wet state [33]. The findings of the examination [34] demonstrate that a decrease in the thermal outlines may be achieved by increasing the surface radiative factor, and a similar pattern of interaction is seen for the surface convection parameter. In addition, liquids containing tripartite nanomaterials exhibit the highest change in temperature. In addition, in comparison with the conventional straight fin, the longitudinal trapezoidal fin has better heat transfer properties, making it the kind of fin that offers the best performance. While in the study [35] obtained that the increased thermal outline in the fin is due to a reduction in the amount of the moist variable, which is essential for the increase.

Because of its relevance to the industry, the nonlinear fin issue has garnered a significant amount of attention in recent years. Porous fins have a broad variety of uses, both in the field of engineering and in daily life. A great number of practical implementations in a variety of manufacturing, electric, and mechanical engineering fields, like gas turbine, motorbike head, aviation machines, vehicles, and heat bowls, employ fin designs to offer greater surface area and, as a consequence, to boost the efficacy of heat transmission. By using wetted porous stretched surfaces, heat transfer rates may be enhanced, and in many cases, these surfaces surpass conventional solid fins in their respective applications. Finally, the significance of this work can be summarized by examining the heat transfer of natural convection on a longitudinal permeable moving fin wetted with a ternary hybridized nanoliquid (Cu–Al$_2$O$_3$–TiO$_2$) numerically and analytically.

2 Governing equations

In the current study, the heat transfer of free convective and radiative consequences on a movement fin with a uniform motion U and a rectangular pattern that is longitudinally porous and moist with a ternary hybrid fluid based on water is modeled. Figure 1 depicts the geometrical structure of the problem under consideration. Assuming that the fin has thickness t, width w, and length l, the Darcy model is used. Furthermore, the fin base is kept at a constant temperature T_b, while the temperature of the surrounding nanofluid is taken into account T_a.

In developing the system strategy, the following presumptions were taken into consideration:

- The Darcy model is adopted.
- T_a denotes the temperature of the ambient nanofluid.
- The base fin has a constant temperature T_b.
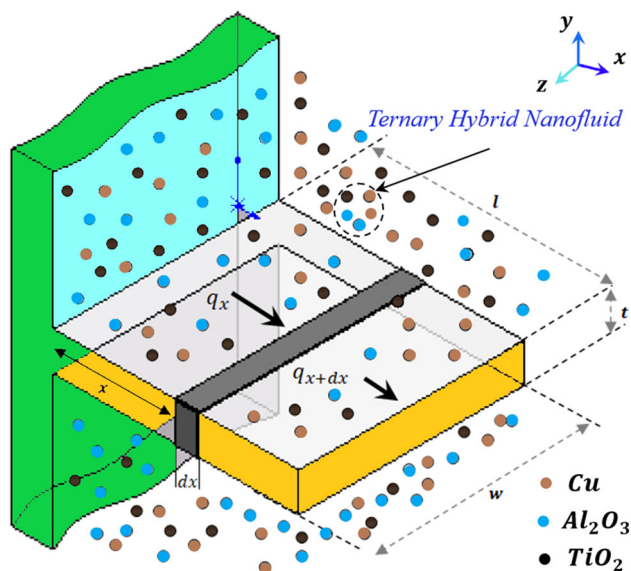
Fig. 1 Schematic representation of the flow geometry

Table 1 Physical properties of ternary hybrid nanofluids [36, 37]

Character	Value
Dynamic viscosity	$\mu_{Thnf} = \mu_f (1-\varphi_1)^{-2.5}(1-\varphi_2)^{-2.5}(1-\varphi_3)^{-2.5}$
Density	$\rho_{Thnf} = (1-\varphi_3)\{(1-\varphi_2)[(1-\varphi_1)\rho_f + \varphi_1\rho_{p_1}] + \varphi_2\rho_{p_2}\} + \varphi_3\rho_{p_3}$
Specific heat	$(\rho C_p)_{Thnf} = (1-\varphi_3)\{(1-\varphi_2)[(1-\varphi_1)(\rho C_p)_f + \varphi_1(\rho C_p)_{p_1}] + \varphi_2(\rho C_p)_{p_2}\} + \varphi_3(\rho C_p)_{p_3}$
Coefficient of thermal expansion	$(\rho\beta)_{Thnf} = (1-\varphi_3)\{(1-\varphi_2)[(1-\varphi_1)(\rho\beta)_f + \varphi_1(\rho\beta)_{p_1}] + \varphi_2(\rho\beta)_{p_2}\} + \varphi_3(\rho\beta)_{p_3}$
Thermal conductivity	$\left.\begin{array}{l}\dfrac{k_{Thnf}}{k_{hnf}} = \dfrac{k_{p_3}+2k_{hnf}-2\varphi_3(k_{hnf}-k_{p_3})}{k_{p_3}+2k_{hnf}-\varphi_3(k_{hnf}-k_{p_3})} \\[6pt] \dfrac{k_{hnf}}{k_{nf}} = \dfrac{k_{p_2}+2k_{nf}-2\varphi_2(k_{nf}-k_{p_2})}{k_{p_2}+2k_{nf}-\varphi_2(k_{nf}-k_{p_2})}, \\[6pt] \dfrac{k_{nf}}{k_f} = \dfrac{k_{p_1}+2k_f-2\varphi_1(k_f-k_{p_1})}{k_{p_1}+2k_f-\varphi_1(k_f-k_{p_1})}.\end{array}\right\}$

- adiabatic fin tip.
- The ambient nanofluid absorbs radiation from the fin's exposed surface.

The energy equation for free convective and radiative terms on a rectangular profiled longitudinal porous moving fin containing ternary hybrid nanofluid is as follows [36, 37]:

$$\frac{d^2T}{dx^2} - \frac{2gK(\rho C_p)_{Thnf}(\rho\beta)_{Thnf}}{\mu_{Thnf}k_{Thnf}t}(T-T_a)^2 - \frac{2\varepsilon\sigma F_{f-a}}{k_{Thnf}t}(T^4-T_a^4)$$
$$- \frac{2h_D i_{fg}(1-\overline{\varphi})(\omega-\omega_a)}{k_{Thnf}t} - \frac{2h(1-\overline{\varphi})(T-T_a)}{k_{Thnf}t} - \frac{(\rho C_p)_{Thnf}U}{k_{Thnf}}\frac{dT}{dx} = 0 \tag{1}$$

where μ_{Thnf}, ρ_{Thnf}, $(C_p)_{Thnf}$, β_{Thnf} and k_{Thnf} are the ternary hybrid nanofluid's dynamic viscosity, density, specific heat with constant pressure, volumetric thermal expansion coefficient, and thermal conductivity.

With the boundary constraints

$$\left.\begin{array}{l} at \ x = 0 \rightarrow T(0) = T_b, \\ at \ x = l \rightarrow \left.\frac{dT}{dx}\right|_{x=l} = 0. \end{array}\right\} \tag{2}$$

Table 1 summarizes the features of a ternary hybridized nanofluid. Whilst Table 2 demonstrates the thermophysical attributes of utilized conventional fluid and nanoparticles.

The heat transmission factor h is given as

$$h = h_a\left(\frac{T-T_a}{T_b-T_a}\right)^n \tag{3}$$

Table 2 Thermophysical attributes of conventional fluid and nanoparticles [12, 13, 38]

Physical attributes	$\rho(\text{kg/m}^3)$	$C_p(\text{J/kgK})$	$k(\text{W/mK})$	$\beta(\text{1/K})$
Pure water H_2O	997.1	4179	0.613	0.00021
Ethylene glycol–water (50–50%)	1063.8	3630	0.37	0.00058
Copper (Cu)	8933	385	401	1.67×10^{-5}
Aluminum oxide (Al_2O_3)	3970	765	40	0.85×10^{-5}
Titanium oxide (TiO_2)	4250	686	8.95	0.9×10^{-5}

Introduce the following similarity transformations:

$$\left. \begin{aligned} \theta &= \frac{T}{T_b}, \\ \theta_a &= \frac{T_a}{T_b}, \\ \eta &= \frac{x}{l}, \\ (\omega - \omega_a) &= b_2(T - T_a), \end{aligned} \right\} \tag{4}$$

We get the dimensionless form by using the above-mentioned similarity transformations:

$$\frac{d^2\theta}{d\eta^2} - Nc \frac{\delta_1 \delta_2}{\frac{1}{\delta_3}}(1-\varphi_1)^{2.5}(1-\varphi_2)^{2.5}(1-\varphi_3)^{2.5}(\theta-\theta_a)^2 - Nr\delta_3(\theta^4 - \theta_a{}^4) - m_2\delta_3\frac{(\theta-\theta_a)^{n+1}}{(1-\theta_a)^n} - Pe\delta_1\delta_3\frac{d\theta}{d\eta} = 0 \tag{5}$$

here,

$$\left. \begin{aligned} \delta_1 &= (1-\varphi_3)\left\{(1-\varphi_2)\left[(1-\varphi_1)+\varphi_1\frac{(\rho C_p)_{p_1}}{(\rho C_p)_f}\right]+\varphi_2\frac{(\rho C_p)_{p_2}}{(\rho C_p)_f}\right\}+\varphi_3\frac{(\rho C_p)_{p_3}}{(\rho C_p)_f}, \\ \delta_2 &= (1-\varphi_3)\left\{(1-\varphi_2)\left[(1-\varphi_1)+\varphi_1\frac{(\rho\beta)_{p_1}}{(\rho\beta)_f}\right]+\varphi_2\frac{(\rho\beta)_{p_2}}{(\rho\beta)_f}\right\}+\varphi_3\frac{(\rho\beta)_{p_3}}{(\rho\beta)_f}, \\ \delta_3 &= \frac{k_f}{k_{Thnf}}, \end{aligned} \right\} \tag{6}$$

The corresponding dimensionless boundary constraints are:

$$\left. \begin{aligned} &at \ \eta = 0 \rightarrow \theta(0) = 1, \\ &at \ \eta = 1 \rightarrow \left. \frac{d\theta}{d\eta}\right|_{\eta=1} = 0. \end{aligned} \right\} \tag{7}$$

where η is the dimensionless axial distance, θ is nondimensional temperature, θ_a is the nondimensional ambient temperature, $Pe = (\rho C_p)_f Ul/k_f$ is the Peclet quantity, $Nr = 2\varepsilon\sigma l^2 T_b{}^3/k_f t$ is the radiative factor, $Nc = 2(\rho\beta)_f gK(\rho C_p)_f T_b l^2/\mu_f k_f t$ is the convective number, $m_2 = \underbrace{2h_a l^2(1-\overline{\varphi})/k_f t}_{m_0} + \underbrace{2h_a l^2 i_{fg}(1-\overline{\varphi})b_2/k_f t(C_p)_f Le^{2/3}}_{m_1}$ is the wet porous number, and n is the power index.

3 Application of ADM

In ADM method [39], Eq. (5) can be written.

$$\mathcal{L}\theta'' = Nc\frac{\delta_1\delta_2}{\frac{1}{\delta_3}}(1-\varphi_1)^{2.5}(1-\varphi_2)^{2.5}(1-\varphi_3)^{2.5}(\theta-\theta_a)^2 + Nr\delta_3(\theta^4-\theta_a^4) + m_2\delta_3\frac{(\theta-\theta_a)^{n+1}}{(1-\theta_a)^n} + Pe\delta_1\delta_3\theta' \tag{8}$$

Here, the differential operator $\mathcal{L}$ and the inverse operator $\mathcal{L}^{-1}$ are specified, respectively, by

$$\left. \begin{aligned} \mathcal{L}_\theta &= \frac{d^2}{d\eta^2}, \\ \mathcal{L}_\theta^{-1}(\blacksquare) &= \int_0^\eta\int_0^\eta(\blacksquare)d\eta d\eta. \end{aligned} \right\} \tag{9}$$

With

$$
\left.
\begin{aligned}
\delta_1 &= (1-\varphi_3)\left\{(1-\varphi_2)\left[(1-\varphi_1)+\varphi_1\frac{(\rho C_p)_{p_1}}{(\rho C_p)_f}\right]+\varphi_2\frac{(\rho C_p)_{p_2}}{(\rho C_p)_f}\right\}+\varphi_3\frac{(\rho C_p)_{p_3}}{(\rho C_p)_f}, \\
\delta_2 &= (1-\varphi_3)\left\{(1-\varphi_2)\left[(1-\varphi_1)+\varphi_1\frac{(\rho\beta)_{p_1}}{(\rho\beta)_f}\right]+\varphi_2\frac{(\rho\beta)_{p_2}}{(\rho\beta)_f}\right\}+\varphi_3\frac{(\rho\beta)_{p_3}}{(\rho\beta)_f}, \\
\delta_3 &= \frac{k_f}{k_{Thnf}}.
\end{aligned}
\right\}
\tag{10}
$$

Operational with $\mathcal{L}^{-1}$ in Eq. (8) and subsequent to exerting boundary constraints on it, we get

$$
\theta = \theta(0)+\theta'(0)\eta+\iint_0^\eta \langle Nc\frac{\delta_1\delta_2}{\frac{1}{\delta_3}}(1-\varphi_1)^{2.5}(1-\varphi_2)^{2.5}(1-\varphi_3)^{2.5}(\theta-\theta_a)^2+Nr\delta_3(\theta^4-\theta_a^4)+m_2\delta_3\frac{(\theta-\theta_a)^{n+1}}{(1-\theta_a)^n}+Pe\delta_1\delta_3\theta'\rangle.
\tag{11}
$$

Alternatively, taking into account the boundary constraints (7), Eq. (11) becomes:

$$
\theta(\eta) = 1+a\eta+\iint_0^\eta \langle Nc\frac{\delta_1\delta_2}{\frac{1}{\delta_3}}(1-\varphi_1)^{2.5}(1-\varphi_2)^{2.5}(1-\varphi_3)^{2.5}(\theta-\theta_a)^2+Nr\delta_3(\theta^4-\theta_a^4)+m_2\delta_3\frac{(\theta-\theta_a)^{n+1}}{(1-\theta_a)^n}+Pe\delta_1\delta_3\theta'\rangle
\tag{12}
$$

In conclusion, the elements of the solution that were derived through the use of the ADM method are outlined below:

$$
\theta(\eta) = \theta_0(\eta)+\iint_0^\eta \langle Nc\frac{\delta_1\delta_2}{\frac{1}{\delta_3}}(1-\varphi_1)^{2.5}(1-\varphi_2)^{2.5}(1-\varphi_3)^{2.5}(\theta-\theta_a)^2+Nr\delta_3(\theta^4-\theta_a{}^4)+m_2\delta_3\frac{(\theta-\theta_a)^{n+1}}{(1-\theta_a)^n}+Pe\delta_1\delta_3\theta'\rangle
\tag{13}
$$

Where.

$$
\theta_0 = 1+a\eta
\tag{14}
$$

The constant a could be determined using boundary conditions. The two components' terms of Adomian polynomials are obtained as follows:

$$
\begin{aligned}
A_0 &= \xi_3 m_2+\frac{1}{\xi_3}\left(\xi_1\xi_2\xi_4 Nc+2\xi_1\xi_2\xi_4 Nca\eta+\xi_1\xi_2\xi_4 Nca^2\eta^2\right)+\xi_3 Nr+\xi_3 m_2 a\eta+\xi_1\xi_3 Pea+6\xi_3 Nra^2\eta^2 \\
&\quad +4\xi_3 Nra\eta+4\xi_3 Nra^3\eta^3+\xi_3 Nra^4\eta^4-\xi_3 m_2\theta_a+\frac{\xi_4}{\xi_3}\left(-2\xi_1\xi_2 Nc\theta_a-2\xi_1\xi_2 Nca\theta_a\eta+\xi_1\xi_2 Nc\theta_a^2\right)-\xi_3 Nr\theta_a^4
\end{aligned}
\tag{15a}
$$

$$
\begin{aligned}
A_1 &= \xi_1\xi_3 Pea+\frac{\xi_1\xi_2\xi_4}{\xi_3}\left(Nc+2Nca\eta+Nca^2\eta^2-2Nc\theta_a-2Nca\eta\theta_a+Nc\theta_a^2\right)+\xi_3\left(m_2+Nr+m2a\eta+4Nra\eta+6Nra^2\eta^2\right. \\
&\quad \left.+4Nra^3\eta^3+Nra^4\eta^4-m_2\theta_a-Nr\theta_a^4+Nr+4Nra\eta+6Nra^2\eta^2+4Nra^3\eta^3+Nra^4\eta^4-Nr\theta_a^4\right)
\end{aligned}
\tag{15b}
$$

Now using ADM, the first terms of the solution are given as.

$$
\begin{aligned}
\theta_1 &= \xi_3\left(\frac{1}{2}m_2\eta^2+\frac{1}{2}Nr\eta^2+\frac{1}{2}\xi_1 Pea\eta^2+\frac{1}{6}m_2 a\eta^3+\frac{2}{3}Nra\eta^3+\frac{1}{2}Nra^2\eta^4+\frac{1}{5}Nra^3\eta^5+\frac{1}{30}Nra^4\eta^6-\frac{1}{2}m_2\eta^2\theta_a-\frac{1}{2}Nr\eta^2\theta_a^4\right) \\
&\quad +\frac{\xi_1\xi_2\xi_4}{\xi_3}\left(\frac{1}{2}Nc\eta^2+\frac{1}{3}Nca\eta^3+\frac{1}{12}Nca^2\eta^4-Nc\eta^2\theta_a-\frac{1}{3}Nca\theta_a\eta^3+\frac{1}{2}Nc\theta_a^2\eta^2\right)
\end{aligned}
\tag{16a}
$$

$$
\begin{aligned}
\theta_2 &= \frac{1}{2}\xi_3 m_2\eta^2+\frac{1}{2\xi_3}\xi_1\xi_2\xi_4 Nc\eta^2+\xi_3 Nr\eta^2+\frac{1}{2}\xi_1\xi_3 Pea\eta^2+\frac{1}{6}\xi_3 m_2 a\eta^3+\frac{1}{3\xi_3}\xi_1\xi_2\xi_4 Nca\eta^3 \\
&\quad +\frac{4}{3}\xi_3 Nra\eta^3+\frac{1}{12\xi_3}\xi_1\xi_2\xi_4 Nca^2\eta^4+\xi_3 Nra^2\eta^4+\frac{2}{5}\xi_3 Nra^3\eta^5+\frac{1}{15}\xi_3 Nra^4\eta^6 \\
&\quad -\frac{1}{2}\xi_3 m_2\eta^2\theta_a-\frac{1}{\xi_3}\xi_1\xi_2\xi_4 Nc\eta^2\theta_a-\frac{1}{3\xi_3}\xi_1\xi_2\xi_4 Nca\eta^3\theta_a+\frac{1}{2\xi_3}\xi_1\xi_2\xi_4 Nc\eta^2\theta_a^2-\xi_3 Nr\eta^2\theta_a^4
\end{aligned}
\tag{16b}
$$

With $\xi_1=\delta_1$, $\xi_2=\delta_2$, $\xi_3=1/\delta_3$, and $\xi_4=\delta_4$.

4 Graphical interpretations and outcomes

The influence of the quantities of the sundry factors on the temperature profile $\theta(\eta)$ is heeded in Figs. 2, 3, 4, 5, 6, 7, 8, 9. The effect of ternary hybrid nanofluid on temperature profile $\theta(\eta)$ of the fin is shown in Fig. 2 when $n = m_2 = 1$, $Nr = Nc = 2$, $\theta_a = 0.3$, $\varphi_{Cu+Al_2O_3+TiO_2} = 0\%, 3\%, 6\%$ and $Pe = 1$. This confirms that from a physical point of view, the solid nanoparticles, if it is increased inside the fluid, raise the thermal energy stored in these molecules, and thus, raise the temperature of the fluid accordingly. Increasing $\varphi_{Cu+Al_2O_3+TiO_2}$ causes a boost in the temperature outline. Figure 3 is presented to see the influence of the nature of the base fluid on the temperature outline $\theta(\eta)$ of the fin. It is noticed that pure water (H_2O) has a higher temperature than the ethylene glycol–water (50–50%) base fluid when $n = m_2 = 1$, $Nr = Nc = 2$, $\theta_a = 0.2$, $\varphi_{Cu+Al_2O_3+TiO_2} = 6\%$ and $Pe = 4$. Physically, the hybrid liquid consisting of ethylene glycol and water has a higher heat transfer rate than pure water. Therefore, we found from the analysis that the pure liquid has a higher temperature than the hybrid liquid.

Figure 4 depicts the result of the power index n on the temperature profile $\theta(\eta)$ of the fin when $m_2 = 1$, $Nr = Nc = 2$, $\theta_a = 0.2$ and $Pe = 1$. It is seen that temperature has an increasing trend for larger values of power index n. The main reason behind this is that by increasing the power index n, the heat transference factor h increases, which in turn increases the temperature outlines $\theta(\eta)$. Figure 5 is outlined to visualize the effect of θ_a on temperature profile $\theta(\eta)$ of the fin when $n = m_2 = 1$, $Nr = 3$, $Nc = 2$, $\varphi_{Cu+Al_2O_3+TiO_2} = 6\%$ and $Pe = 1$. It is remarked that the temperature for the increasing parametric amounts of θ_a is increased. This implies that as the surrounding temperature rises, heat transference from the fin surface to the surrounding environment diminishes. Rising the temperature of the ambient medium θ_a raises the temperature of the fluid because of the convection process, which in turn slows down the rate of heat transport.

Figure 6 is plotted to perceive the influence of the Peclet number on the temperature profile $\theta(\eta)$ of the fin when $n = m_2 = 1$, $Nr = Nc = 2$, $\varphi_{Cu+Al_2O_3+TiO_2} = 6\%$ and $\theta_a = 0.2$. It is found that an increase in Peclet quantity Pe shows an upsurge in temperature profile $\theta(\eta)$. On the other side, the greater the speed, the less time there is for the fin to interact with its environment. As a result, as Pe increases, heat transfer diminishes. Whereas, from a physical point of view, the Peclet amount Pe depends on the heat capacity $(\rho C_p)_f$. The greater heat capacity causes in enhance the Peclet quantity. On the contrary, regarding the thermal conductivity of the fluid k_f, this causes an enhancement in the temperature outlines. Figure 7 displays the consequences of m_2 (the wet porous variable) on the temperature outline $\theta(\eta)$ of the fin when $n = 1$, $\varphi_{Cu+Al_2O_3+TiO_2} = 6\%$, $Nr = Nc = 2$, $\theta_a = 0.2$ and $Pe = 2$. Here, we note that with a surge in m_2, the temperature declines. Physically, the higher number of wet porous results in a great heat transference rate, and thus, the temperature of the fluid begins to decline gradually. Figure 8 depicts the consequences of convective parameters on the temperature outlines $\theta(\eta)$ of fins when $n = m_2 = 1$, $\varphi_{Cu+Al_2O_3+TiO_2} = 6\%$, $Nr = 2$, $\theta_a = 0.2$ and

Fig. 2 Effect of $\varphi_{Cu+Al_2O_3+TiO_2}$ on $\theta(\eta)$ when $n = m_2 = 1$, $Nr = Nc = 2$, $\theta_a = 0.3$ and $Pe = 1$
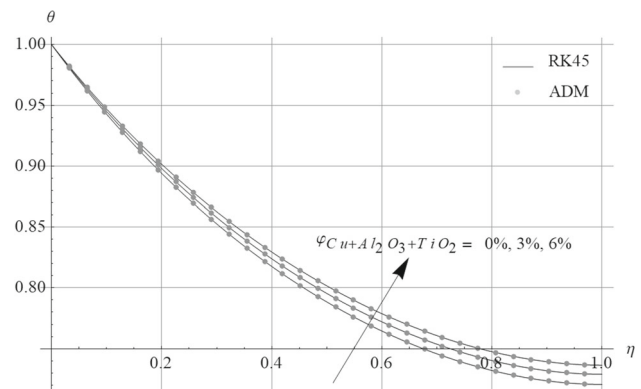

Fig. 3 Effect of nature of the base fluid on $\theta(\eta)$ when $n = m_2 = 1$, $\varphi_{Cu+Al_2O_3+TiO_2} = 6\%$, $Nr = Nc = 2$, $\theta_a = 0.2$ and $Pe = 4$
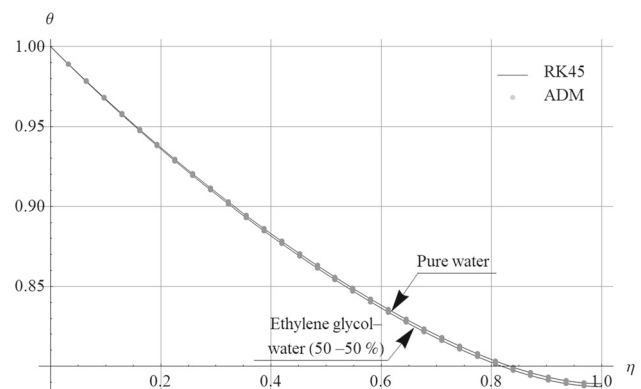
Fig. 4 Effect of power index n on $\theta(\eta)$ when $m_2 = 1$, $\varphi_{Cu+Al_2O_3+TiO_2} = 6\%$, $Nr = Nc = 2$, $\theta_a = 0.2$ and $Pe = 1$
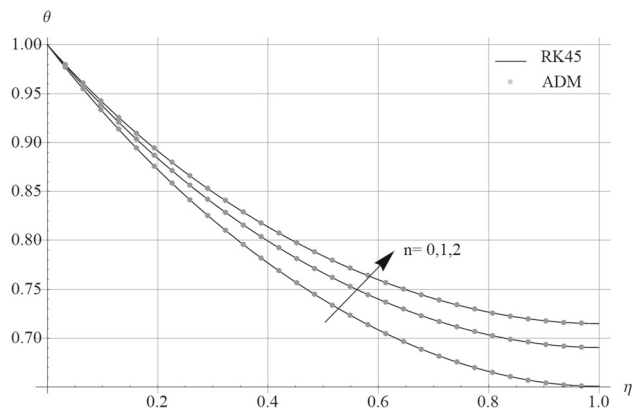

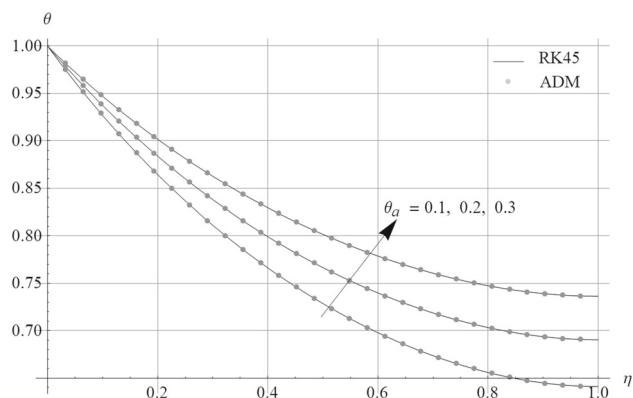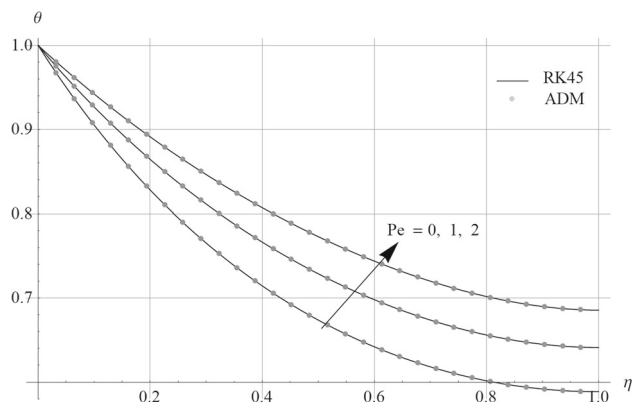**Fig. 5** Consequence of θ_a on $\theta(\eta)$ when $n = m_2 = 1$, $Nr = 3$, $Nc = 2$, $\varphi_{Cu+Al_2O_3+TiO_2} = 6\%$ and $Pe = 1$

Fig. 6 Consequence of Pe on $\theta(\eta)$ when $n = m_2 = 1$, $Nr = Nc = 2$, $\varphi_{Cu+Al_2O_3+TiO_2} = 6\%$ and $\theta_a = 0.2$

$Pe = 1$. There is a decrease in $\theta(\eta)$ of the fin when Nc increases. The realize of radiative variable Nr on the temperature outline is shown in Fig. 9 when $n = 0$, $m_2 = 1$, $\varphi_{Cu+Al_2O_3+TiO_2} = 6\%$, $Nc = 1$, $\theta_a = 0.1$ and $Pe = 1$. It is observed that a rise in Nr produces a boost in the temperature profile. The improvements in the convective number and radiative parameter raise the rate of heat transport inside the fluid because of the work of the wetted fin with the trihybrid nanofluid, which makes the thermal energy stored inside the fluid begin to dissipate, which reduces the temperature of the nanofluid. Effects of ambient temperature and nature of nanofluid (i.e., ternary hybrid nanofluid, hybrid nanofluid, and Pure water) on a thermal gradient are shown in Fig. 10 when $n = m_2 = 1$, $Nr = Nc = 2$, $\varphi_{Cu+Al_2O_3+TiO_2} = 6\%$ and $Pe = 1$. As visualized, the thermal gradient decreases with the augment of both ambient temperature and the nature of nanofluid, Therefore, in the working fluid, we discover that a water-based ternary hybrid nanofluid (Cu + Al$_2$O$_3$ + TiO$_2$) exhibits promising heat transfer. In addition, it can be said that one of the most important results of the current study is that when ethylene glycol is added to pure water to make the base fluid as a hybrid fluid, this results in a better heat transport rate than in the case of pure water only as conventional fluid. This result can be applied as a basis for industrial cooling processes in addition to the work of the fin during cooling.

The comparison of the water-based ternary hybrid nanofluid (Cu + Al$_2$O$_3$ + TiO$_2$/H$_2$O) with Ethylene glycol–water (50–50%)-based ternary hybrid nanofluid (Cu + Al$_2$O$_3$ + TiO$_2$/H$_2$O (50%)-C$_2$H$_6$O$_2$(50%)) is highlighted in Fig. 11 when $n = m_2 = 1$,

Fig. 7 Consequence of m_2 on $\theta(\eta)$ when $n = 1$, $\varphi_{\text{Cu+Al}_2\text{O}_3\text{+TiO}_2} = 6\%$, $Nr = Nc = 2$, $\theta_a = 0.2$ and $Pe = 2$
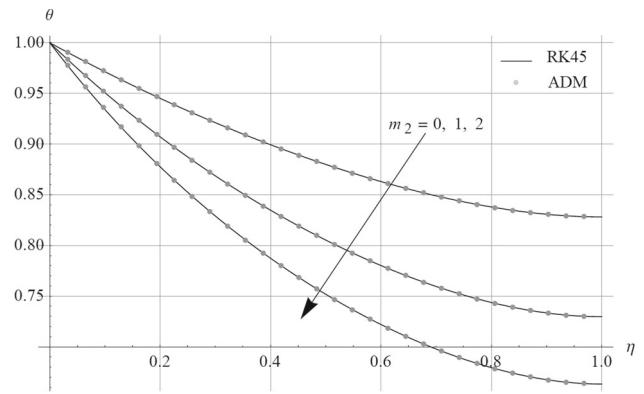

Fig. 8 Effect of Nc on $\theta(\eta)$ when $n = m_2 = 1$, $\varphi_{\text{Cu+Al}_2\text{O}_3\text{+TiO}_2} = 6\%$, $Nr = 2$, $\theta_a = 0.2$ and $Pe = 1$
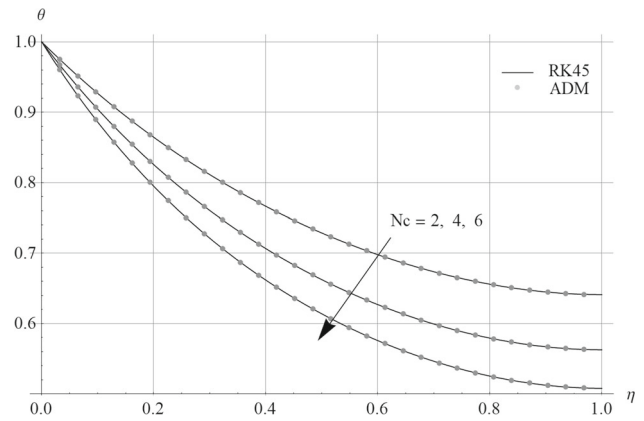

Fig. 9 Effect of Nr on $\theta(\eta)$ when $n = 0$, $m_2 = 1$, $\varphi_{\text{Cu+Al}_2\text{O}_3\text{+TiO}_2} = 6\%$, $Nc = 1$, $\theta_a = 0.1$ and $Pe = 1$
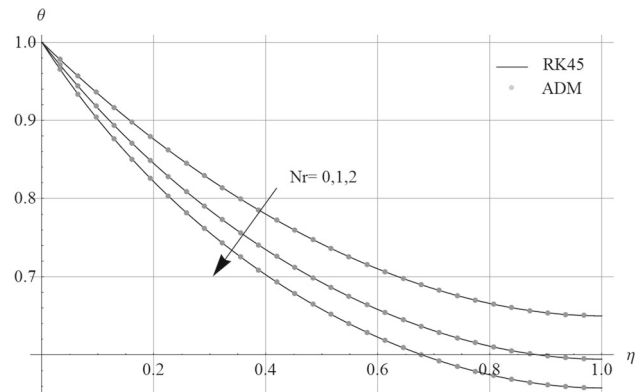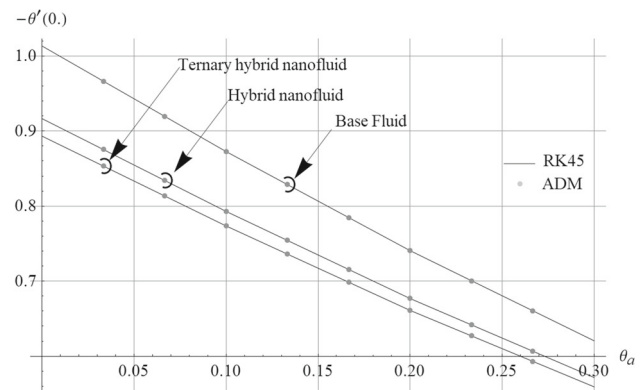

Fig. 10 Effects of θ_a and nature of nanofluid on $-\theta'(\eta)$ when $n = m_2 = 1$, $Nr = Nc = 2$, $\varphi_{\text{Cu+Al}_2\text{O}_3\text{+TiO}_2} = 6\%$ and $Pe = 1$

$Nr = Nc = 2$, $\theta_a = 0.2$ and $Pe = 1$. When compared to Ethylene glycol–water (50–50%)-based, water-based exhibits greater heat transport. Alternatively, The thermic gradient decreases with the augment of the volume fraction of nanoparticle $\varphi_{\text{Cu}-\text{Al}_2\text{O}_3-\text{TiO}_2}$.

Fig. 11 Effects of $\varphi_{Cu+Al_2O_3+TiO_2}$ and nature of the base fluid on $-\theta'(\eta)$ when $n = m_2 = 1$, $Nr = Nc = 2$, $\theta_a = 0.2$ and $Pe = 1$
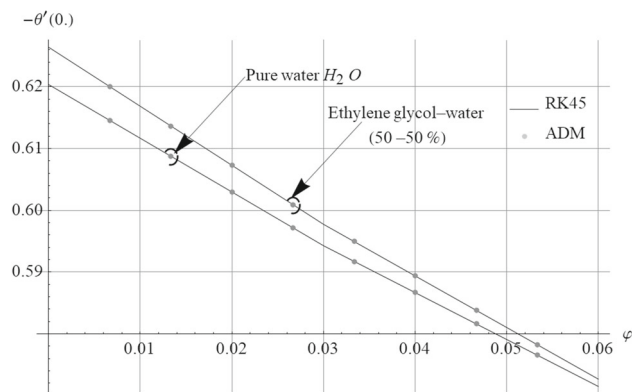

Fig. 12 Order of approximation of ADM solution when $n = m_2 = 1$, $Nr = Nc = 1$, $\varphi_{Cu+Al_2O_3+TiO_2} = 6\%$, $\theta_a = 0.1$ and $Pe = 1$
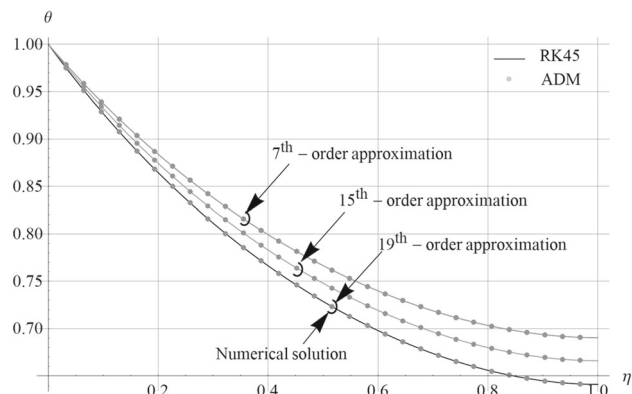

Fig. 13 Comparison among the obtained outcomes and HAM-based Mathematica package calculations $\theta(\eta)$ when $n = 1$, $m_2 = 2$, $\varphi_{Cu+Al_2O_3+TiO_2} = 6\%$, $Nr = Nc = 2$, $\theta_a = 0.1$ and $Pe = 2$
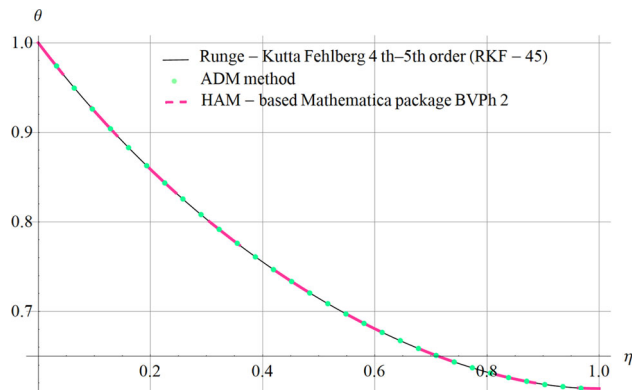

Table 3 The comparison between ADM results and HAM solution for $\theta(\eta)$ when $n = 1$, $m_2 = Nr = Nc = 2$, $\theta_a = 0.1$, $\varphi_{Cu+Al_2O_3+TiO_2} = 0\%$, and $Pe = 2$

η	$\theta(\eta)$	
	ADM outcomes	HAM outcomes
0.0	1.000000000	1.0000000000
0.2	0.8468376170	0.8468376190
0.4	0.7372376720	0.7372376730
0.6	0.6598932654	0.6598932656
0.8	0.6107846181	0.6107846184
1.0	0.5925316609	0.5925316620

The converges of ADM method are illustrated in Fig. 12 for temperature profile $\theta(\eta)$ of the fin when $n = m_2 = 1$, $Nr = Nc = 1$, $\varphi_{Cu+Al_2O_3+TiO_2} = 6\%$, $\theta_a = 0.1$ and $Pe = 1$. It is observed that the ADM analytical solution converges quickly to the RK45 numerical solution at the 19th-order of approximation. When $n = 1$, $m_2 = 2$, $\varphi_{Cu+Al_2O_3+TiO_2} = 6\%$, $Nr = Nc = 2$, $\theta_a = 0.1$ and $Pe = 2$, the comparison of the HAM-based Mathematica software BVPh 2 with the ADM approach and the Runge–Kutta–Fehlberg fourth–fifth order (RKF-45) is shown in Fig. 13 and Table 3. The findings show that there is a remarkable degree of concordance between the two sets of data.

5 Concluding remarks

The following are the primary important points of the requested issue:

- Increasing, $\varphi_{\mathrm{Cu+Al_2O_3+TiO_2}}$, power index n, ambient temperature θ_a, and Peclet quantity Pe increases temperature profile $\theta(\eta)$.
- Improving wet porous variable m_2, convective variable Nc, and radiation factor Nr decreases temperature profile $\theta(\eta)$.
- Pure water has a higher temperature than the ethylene glycol–water (50–50%) base fluid.
- The thermal gradient is found to decrease by increasing $\varphi_{\mathrm{Cu+Al_2O_3+TiO_2}}$ and θ_a.
- Comparisons and convergence tests have proven that the HAM approach is highly resilient and trustworthy.

Data Availability Statement The manuscript has no associated data.

Declarations

Conflict of interest The authors have no conflicts of interest to declare.

References

1. M.S. Abdel-Wahed, E.M. Elsaid, Magnetohydrodynamic flow and heat transfer over a moving cylinder in a nanofluid under convective boundary conditions and heat generation. Thermal Sci. **23**(6B), 3785–3796 (2019)
2. N.T. Eldabe, E.M. Elbashbeshy, T.G. Emam, E.M. Elsaid, Effect of thermal radiation on heat transfer over an unsteady stretching surface in a micropolar fluid with variable heat flux. Int. J. Heat Technol. **30**, 93–98 (2012)
3. A.M. Morad, E.S. Selima, A.K. Abu-Nab, Thermophysical bubble dynamics in N-dimensional Al_2O_3/H_2O nanofluid between two-phase turbulent flow. Case Stud. Therm. Eng. **28**, 101527 (2021)
4. K. Das, Slip flow and convective heat transfer of nanofluids over a permeable stretching surface. Comput. Fluids **64**, 34–42 (2012)
5. M.R. Eid, M.A. Ahmed, F.M. Hady, A nanofluid flow in a non-linear stretching surface saturated in a porous medium with yield stress effect. Appl. Math. Inf. Sci. Lett. **2**(2), 43–51 (2014)
6. T. Sajid, A. Ayub, S.Z. Shah, W. Jamshed, M.R. Eid, E.M. Tag El Din, R. Irfan, S.M. Hussain, Trace of chemical reactions accompanied with arrhenius energy on ternary hybridity nanofluid past a wedge. Symmetry **14**, 1850 (2022)
7. S. Munawar, N. Saleem, Mixed convective cilia triggered stream of magneto ternary nanofluid through elastic electroosmotic pump: a comparative entropic analysis. J. Mol. Liq. **352**, 118662 (2022)
8. M. Haneef, H.A. Madkhali, A. Salmi, S.O. Alharbi, M.Y. Malik, Numerical study on heat and mass transfer in Maxwell fluid with tri and hybrid nanoparticles. Int. Commun. Heat Mass Transf. **135**, 106061 (2022)
9. W. Xiu, S. Saleem, W. Weera, U. Nazi, Cattaneo-christove thermal flux in reiner philippoff martial under action of variable lorentz force employing tri-hybrid nanomaterial approach. Case Stud. Therm. Eng. **38**, 102267 (2022)
10. A.K. Abu-Nab, A.M. Morad, E.S. Selima, Impact of magnetic-field on the dynamic of gas bubbles in N-dimensions of non-Newtonian hybrid nanofluid: analytical study. Phys. Scr. **97**, 105202 (2022)
11. E.M. Elsaid, M.S. Abdel-wahed, Mixed convection hybrid-nanofluid in a vertical channel under the effect of thermal radiative flux. Case Stud. Therm. Eng. **25**, 100913 (2021)
12. E.M. Elsaid, M.S. Abdel-wahed, MHD mixed convection Ferro Fe_3O_4/Cu-hybrid-nanofluid runs in a vertical channel. Chin. J. Phys. **76**, 269–282 (2022)
13. E.M. Elsaid, K.S. AlShurafat, Impact of Hall current and Joule heating on a rotating hybrid nanofluid over a stretched plate with nonlinear thermal radiation. J. Nanofluids **12**, 1–9 (2023)
14. B.J. Gireesha, G. Sowmya, M.I. Khan, H.F. Öztop, Flow of hybrid nanofluid across a permeable longitudinal moving fin along with thermal radiation and natural convection. Comput. Meth. Prog. Biomed. **185**, 105166 (2020)
15. N. Talbi, M. Kezzar, M. Malaver, I. Tabet, M.R. Sari, A. Metatla, M.R. Eid, Increment of heat transfer by graphene-oxide and molybdenum-disulfide nanoparticles in ethylene glycol solution as working nanofluid in penetrable moveable longitudinal fin. Waves Random Complex Media (2022). https://doi.org/10.1080/17455030.2022.2026527
16. M. Kezzar, I. Tabet, M.R. Eid, A new analytical solution of longitudinal fin with variable heat generation and thermal conductivity using DRA. Eur. Phys. J. Plus **135**, 120 (2020)
17. G. Sowmya, B.J. Gireesha, S. Sindhu, B.C. Prasannakumara, Investigation of Ti6Al4V and AA7075 alloy embedded nanofluid flow over longitudinal porous fin in the presence of internal heat generation and convective condition. Commun. Theore. Phys. **72**, 025004 (2020)
18. J.S. Goud, S. Pudhari, R.V. Kumar, K.T. Kumar, U. Khan, Z. Raizah, H.S. Gill, A.M. Galal, Role of ternary hybrid nanofluid in the thermal distribution of a dovetail fin with the internal generation of heat. Case Stud. Therm. Eng. **35**, 102113 (2022)
19. S. Hosseinzadeh, K. Hosseinzadeh, A. Hasibi, D. Ganji, Thermal analysis of moving porous fin wetted by hybrid nanofluid with trapezoidal, concave parabolic and convex cross sections. Case Stud. Therm. Eng. **30**, 101757 (2022)
20. S. Gouran, S. Ghasemi, S. Mohsenian, Effect of internal heat source and non-independent thermal properties on a convective–radiative longitudinal fin. Alex. Eng. J. **61**, 8545–8554 (2022)
21. M.A. Sadiq, T. Hayat, Darcy-Forchheimer flow of magneto Maxwell liquid bounded by convectively heated sheet. Results Phys. **6**, 884–890 (2016)
22. A. Ibragimov, T.T. Kieu, An expanded mixed finite element method for generalized Forchheimer flows in porous media. Comput. Math. Appl. **72**, 1467–1483 (2016)
23. Z. Shah, A. Dawar, S. Islam, I. Khan, D.L.C. Ching, Darcy-Forchheimer flow of radiative carbon nanotubes with microstructure and inertial characteristics in the rotating frame. Case Stud. Therm. Eng. **12**, 823–832 (2018)
24. T. Hayat, S.R. Saif, Numerical study for Darcy-Forchheimer flow due to a curved stretching surface with Cattaneo-Christov heat flux and homogeneous/heterogeneous reactions. Results Phys. **7**, 2886–2892 (2017)

25. M.I. Khan, F. Alzahrani, A. Hobiny, Z. Ali, Estimation of entropy optimization in Darcy-Forchheimer flow of Carreau-Yasuda fluid (non-Newtonian) with first order velocity slip. Alex. Eng. J. **59**, 3953–3962 (2020)

26. Y.-X. Li, T. Muhammad, M. Bilal, M.A. Khan, A. Ahmadian, B.A. Pansera, Fractional simulation for Darcy-Forchheimer hybrid nanoliquid flow with partial slip over a spinning disk. Alex. Eng. J. **60**, 4787–4796 (2021)

27. E.M. Elsaid, E.M. Abdel-Aal, Darcy-Forchheimer flow of a nanofluid over a porous plate with thermal radiation and Brownian motion. J. Nanofluid **12**, 1 (2023)

28. R. Varun Kumar, G. Sowmya, B. Prasannakumara, Significance of non-Fourier heat conduction in the thermal analysis of a wet semi-spherical fin with internal heat generation. Waves Random Complex Media (2022). https://doi.org/10.1080/17455030.2022.2134601

29. G. Sowmya, M.M. Lashin, M.I. Khan, R.V. Kumar, K. Jagadeesha, B. Prasannakumara, K. Guedri, O.T. Bafakeeh, E.S. Mohamed Tag-ElDin, A.M. Galal, Significance of convection and internal heat generation on the thermal distribution of a porous dovetail fin with radiative heat transfer by spectral collocation method. Micromachines **13**(8), 1336 (2022)

30. J.S. Goud, P. Srilatha, R.V. Kumar, G. Sowmya, F. Gamaoun, K. Nagaraja, J.S. Chohan, U. Khan, S.M. Eldin, Heat transfer analysis in a longitudinal porous trapezoidal fin by non-Fourier heat conduction model: an application of artificial neural network with Levenberg–Marquardt approach. Case Stud. Therm. Eng. **49**, 103265 (2023)

31. G. Sowmya, R.S.V. Kumar, Y. Banu, Thermal performance of a longitudinal fin under the influence of magnetic field using Sumudu transform method with pade approximant (STM-PA). ZAMM-J. Appl. Math. Mech. (2023). https://doi.org/10.1002/zamm.202100526

32. R. Kumar, G. Sowmya, R. Kumar, Execution of probabilists' Hermite collocation method and regression approach for analyzing the thermal distribution in a porous radial fin with the effect of an inclined magnetic field. Eur. Phys. J. Plus **138**(5), 1–19 (2023)

33. A. Abdulrahman, F. Gamaoun, R.V. Kumar, U. Khan, H.S. Gill, K. Nagaraja, S.M. Eldin, A.M. Galal, Study of thermal variation in a longitudinal exponential porous fin wetted with TiO_2-SiO_2/hexanol hybrid nanofluid using hybrid residual power series method. Case Stud. Therm. Eng. **43**, 102777 (2023)

34. F. Gamaoun, N.M. Said, R. Makki, R.V. Kumar, G. Sowmya, B. Prasannakumara, R. Kumar, Energy transfer of a fin wetted with ZnO-SAE 50 nanolubricant: an application of α-parameterized differential transform method. Case Stud. Therm. Eng. **40**, 102501 (2022)

35. R. Varun Kumar, G. Sowmya, A novel analysis for heat transfer enhancement in a trapezoidal fin wetted by $MoS_2+Fe_3O_4+NiZnFe_2O_4$-methanol based ternary hybrid nanofluid. Waves Random Complex Media (2022). https://doi.org/10.1080/17455030.2022.2134605

36. B.J. Gireesha, G. Sowmya, S. Sindhu, Analysis of thermal behavior of moving longitudinal porous fin wetted with water-based SWCNTs and MWCNTs. Heat Transf. **2020**, 1–15 (2020)

37. G. Sowmya, B.J. Gireesha, H. Berrehal, An unsteady thermal investigation of a wetted longitudinal porous fin of different profiles. J. Therm. Anal. Calorim. **143**, 2463–2474 (2021)

38. E.M. Elsaid, M.S. Abdel-wahed, Impact of hybrid nanofluid coolant on the boundary layer behavior over a moving cylinder: numerical case study. Case Stud. Therm. Eng. **25**, 100951 (2021)

39. C.M. Ayeche, M. Kezzar, M.R. Sari, M.R. Eid, Analytical ADM study of time-dependent hydromagnetic flow of biofluid over a wedge. Indian J. Phys. **95**(12), 2769–2784 (2021)